Simultaneous Determination of Photoreaction Dynamics and Energetics Using Pulsed, Time-Resolved Photoacoustic Calorimetry

Jeanne E. Rudzki, Joshua L. Goodman, and Kevin S. Peters*

Contribution from the Department of Chemistry, University of Colorado, Boulder, Colorado 80309. *Received June 14, 1985*

Abstract: Pulsed, time-resolved photoacoustic calorimetry has been expanded to allow the simultaneous determination of the dynamics and energetics of photoinitiated reactions. Up to three decays may be analyzed assuming either simultaneous or sequential first-order kinetics. With the present experimental apparatus employing a 1 MHz transducer, transient lifetimes from ~50 ns to ~50 μs may be resolved. Energetics are computed from the fraction of the photon energy released thermally by the decay of the transient of interest. The technique has been applied to the quenching of the benzophenone triplet state by 2,5-dimethylhexa-2,4-diene and the Norrish type II photocleavage of valerophenone, giving kinetic and thermodynamic results in excellent agreement with literature values.

I. Introduction

Pulsed, time-resolved photoacoustic calorimetry is a technique which has been used to determine the reaction enthalpy for photoinitiated reactions generating either stable products or transient intermediates.[1-4] In the present work we show how photoacoustic measurements can provide information on the dynamics of photochemical reactions simultaneously with the calorimetric information. Because photoacoustic calorimetry measures thermal relaxation processes, reaction pathways involving intermediates without easily-monitored chromophores can be detected.

We present herein a brief description of the use of photoacoustic calorimetry to date and the limitations of the technique which prompted the development of photoacoustic waveform deconvolution. The theory of waveform deconvolution is then presented in detail, along with computer model studies to demonstrate the range and limitations of the method. Finally, the technique is applied to the quenching of the benzophenone triplet state by dienes and the Norrish type II photoreaction of valerophenone. These results illustrate the applicability of the technique to simple organic photoreactions.

II. Background

The foundations of pulsed laser photoacoustic calorimetry were established by Rothberg and co-workers.[1] For photochemically simple systems with known quantum yields and kinetics, the photoacoustic signal is given by

$$S = k\phi_h E_p(1 - 10^{-A}) \quad (1)$$

where S is the voltage representing the photoacoustic wave amplitude, A is the sample absorbance, E_p is the incident laser pulse energy, and ϕ_h is the fraction of the photon energy released nonradiatively in thermal relaxation processes. The variable k is an empirically determined proportionality constant relating deposited energy to photoacoustic signal amplitude. Rothberg and co-workers[1] demonstrated how eq 1 can be used to determine ϕ_h for samples of interest, thus allowing the measurement of the enthalpy of formation of the metastable radical pair from triplet benzophenone and aniline. The measured enthalpy of formation was in agreement with that calculated by a thermochemical cycle from known heats of formation. Photoacoustic calorimetry was then applied to a variety of systems to determine, for example, the heat of reaction for the formation of diphenylcarbene from diphenyldiazomethane[2] and the heat of formation of diphenylcyclopropenone.[4]

As with any new technique, pulsed laser photoacoustic calorimetry has evolved considerably since it was first developed. Continuous redesign of the experiment has changed the photolysis energy requirement from several hundred μJ[3] to 10 μJ.[4] Early studies[1-3] used the approximation that $(1 - 10^{-A}) \sim A$ for "low" sample absorbances so that the photoacoustic signal S was stated to be proportional to A rather than $(1 - 10^{-A})$. This approximation does, in fact, lead to nonlinearity in the results and contributes to the overall error in those early enthalpy measurements. Even with lower pulse energies, thus minimizing the potential for multiphoton artifacts, and using the proper expression for the photoacoustic signal, eq 1, Grabowski and co-workers[4] were still not able to quote error limits of less than ±4 kcal/mol. A large portion of the uncertainty in the measurement is due to the uncertainty in the ϕ_h values for the molecules used as calorimetry standards. The ϕ_h values for the standards are calculated from literature values for fluorescence quantum yields, average fluorescence frequencies, intersystem-crossing quantum yields, triplet lifetimes, and triplet energies[1-4] and are subject to the cumulative errors of those values.

More fundamental limitations of the technique exist. To state any reaction enthalpy with certainty, it is necessary to know precisely the quantum yield for the formation of the product.[3] To use the simple technique expressed by eq 1 for photoacoustic calorimetry with a 1-μs transducer, it is necessary that the reactive intermediate of interest be formed in less than 1 ns and have a lifetime of greater than 1 ms. The following section shows how the intermediate processes can be separated from the fast (<1 ns) and slow (>1 ms) heat depositions so that the 1 ns/1 ms rule is no longer a requirement for doing photoacoustic calorimetry; and, photoacoustic calorimetry may be used to obtain simultaneously both the kinetics and thermodynamics of a photoinitiated reaction. The requirement for the known quantum yield for photoreaction remains but only for the thermodynamic information. The reaction kinetics, once initiated, are independent of quantum yield for photoinitiation.

III. Theory

The theory of pulsed, time-resolved photoacoustic calorimetry relies on the varying response of the transducer to heat depositions occurring on different time scales. Rothberg and co-workers[1] found that all "fast" heat depositions look the same to the transducer; all "slow" depositions are ignored; and between the fast and slow domains there exists an intermediate regime in which the transducer response tracks the profile of heat deposition. In principle, one can deduce the history of heat deposition in a sample

(1) Rothberg, L. J.; Simon, J. D.; Bernstein, M.; Peters, K. S. *J. Am. Chem. Soc.* **1983**, *105*, 3464.
(2) Simon, J. D.; Peters, K. S. *J. Am. Chem. Soc.* **1983**, *105*, 5156.
(3) Bernstein, M.; Simon, J. D.; Peters, K. S. *Chem. Phys. Lett.* **1983**, *100*, 241.
(4) Grabowski, J. J.; Simon, J. D.; Peters, K. S. *J. Am. Chem. Soc.* **1984**, *106*, 4615.

0002-7863/85/1507-7849$01.50/0

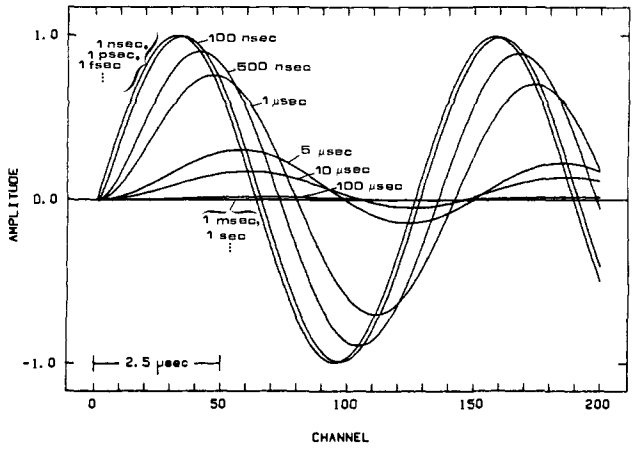

Figure 1. Convolution of transient heat decays (variable τ) with transducer ($\upsilon = 10^6$ Hz, $\tau_0 = 1$ ms) as modeled by eq 1.

by analysis of the photoacoustic signal, making it possible to obtain both calorimetric and dynamic information about a system.

To understand how the transducer signal reflects the original heat deposition profile in space and time, Rothberg and coworkers[1] initially modeled the photoacoustic experiment with a point source of heat and a point detector (transducer). The point source of heat was given the form $(1/\tau)\exp(-t/\tau)$ where τ is the lifetime of the transient and the pre-exponential term $1/\tau$ is a normalization factor so that the total heat deposition of the transient is independent of τ. The transducer was defined to be sensitive to longitudinal displacement waves and was modeled as an underdamped harmonic oscillator. The Green's function analysis, involving the time domain convolution of the heat source and detector, gave the result

$$V(t) = \frac{h_0 A}{4\pi r_0} \frac{\upsilon/\tau}{\upsilon^2 + (1/\tau')^2} e^{-t/\tau} - e^{-t/\tau_0}\left[\cos(\upsilon t) - \frac{1}{\upsilon\tau'}\sin(\upsilon t)\right] \quad (2)$$

where $V(t)$ = detector response, $h_0A/\pi r_0$ = constant υ = characteristic oscillation frequency of the transducer (e.g., 10^6 Hz), τ_0 = relaxation time of the transducer (e.g., 1 ms), τ = lifetime of the transient, and $1/\tau' = 1/\tau - 1/\tau_0$.

Equation 2 is modeled in Figure 1, and forms the basis for photoacoustic calorimetry. All short-lived transients (1 ns, 1 ps, 1 fs, ...) give rise to the same photoacoustic waveform. Thus, the signal due to short-lived transients is independent of τ, which is reasonable, because the transducer cannot discriminate between pressure waves which are much faster than its response time, $1/\upsilon$. All long-lived transients (1 ms, 1 s, ...) give rise to virtually no photoacoustic signal. Dramatically less signal amplitude is induced by the same net heat deposition on time scales long compared to $1/\upsilon$ because the detector's sinusoidal "impulse" responses associated with different time slices of the arriving pressure waves can get out of phase in time $1/2\upsilon$ and destructively interfere. In the intermediate regime (1 ns $< \tau <$ 1 ms), the photoacoustic waveform is reduced in amplitude and appears to be phase shifted with respect to the waveform resulting from fast ($\tau <$ 1 ns) heat decays. In this regime, each value of τ gives rise to a unique waveform.

For n simultaneous reactions, we have shown,[5] using Fourier transform analysis, that

$$V(t) = \sum_{k=1}^{n} K'\phi_k \frac{\upsilon/\tau_k}{\upsilon^2 + (1/\tau_k')^2} e^{-t/\tau_k} - e^{-t/\tau_0}\left[\cos(\upsilon t) - \frac{1}{\upsilon\tau_k'}\sin(\upsilon t)\right] \quad (3)$$

where $V(t)$, υ, and τ_0 are defined as for eq 2, and K' = constant, ϕ_k = amplitude factor for transient k, τ_k = lifetime of transient k, and $1/\tau_k' = 1/\tau_k - 1/\tau_0$. Equation 3 means that the observed acoustic wave resulting from the heat depositions of several simultaneous transient decays is the sum of the waveforms which would be observed from each of the decays individually. A similar analysis has been carried out for n sequential reactions.[5]

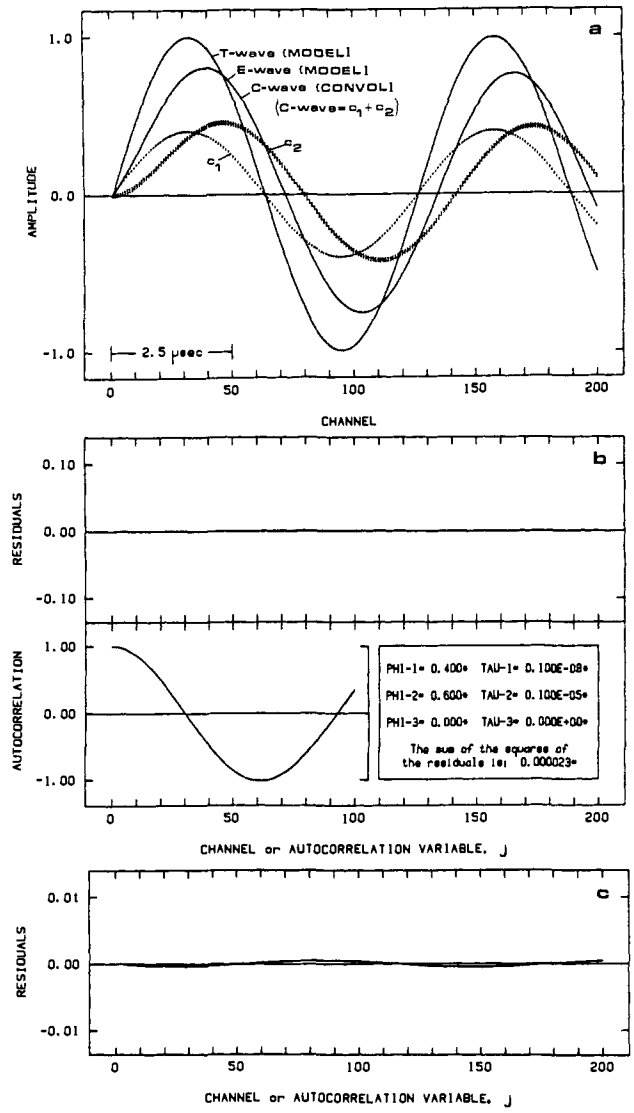

Figure 2. Model studies of waveform deconvolution. The transducer wave (T wave) was modeled with $\phi = 1.0$, $\tau = 1$ ns; the experimental wave (E wave) with two simultaneous decays represented by $\phi_1 = 0.40$, $\tau_1 = 1.0$ ns and $\phi_2 = 0.60$, $\tau_2 = 1.0$ μs; and the convoluted wave (C wave) with the same parameters as the E wave. (a) Waveforms; (b) residuals and autocorrelation of the residuals; (c) residuals on an expanded scale.

Deconvolution of Photoacoustic Waveforms. The goal of time-resolved photoacoustic calorimetry is to obtain the amplitude factor, ϕ_k, and the lifetime of the transient, τ_k. The experimental waveform, $C_{exptl}(t)$, is the convolution of the time-dependent heat source, $E(t)$, with the transducer function, $T(t)$. The transducer

$$C_{exptl}(t) = E(t) * T(t)$$

response function, $T(t)$, may be obtained by generating an impulse function by photoexciting a calibration compound which decays within 1 ns.

The procedure for deconvolution involves determining an $E(t)$ for a set of ϕ_k, τ_k, and then carrying out the convolution of $E(t)$ with $T(t)$ to produce $C_{calcd}(t)$. The calculated $C_{calcd}(t)$ is compared to the experimental $C_{exptl}(t)$ by evaluation of the sum of the squares of residuals. ϕ_k and τ_k are then varied to minimize the residuals. The details of this procedure can be found in ref 5.

IV. Model Studies

Deconvolution of photoacoustic waveforms is achieved by a computer program[5] which also allows model photoacoustic studies by means of eq 3. By giving the transducer parameters as $\upsilon = 10^6$ Hz and $\tau_0 = 1$ ms, a model system is set up which gives

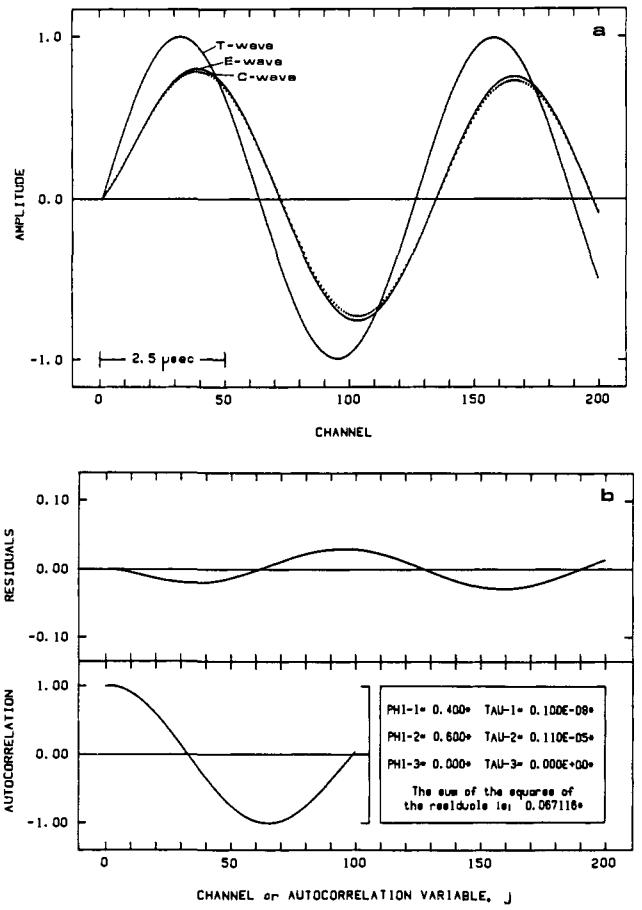

Figure 3. Model studies of waveform deconvolution. The T wave and E wave (solid lines) are identical with those of Figure 2. The C wave (dotted line) was calculated by using an incorrect choice for τ_2 (1.1 rather than 1.0 μs). (a) Waveforms; (b) residuals and autocorrelation of residuals.

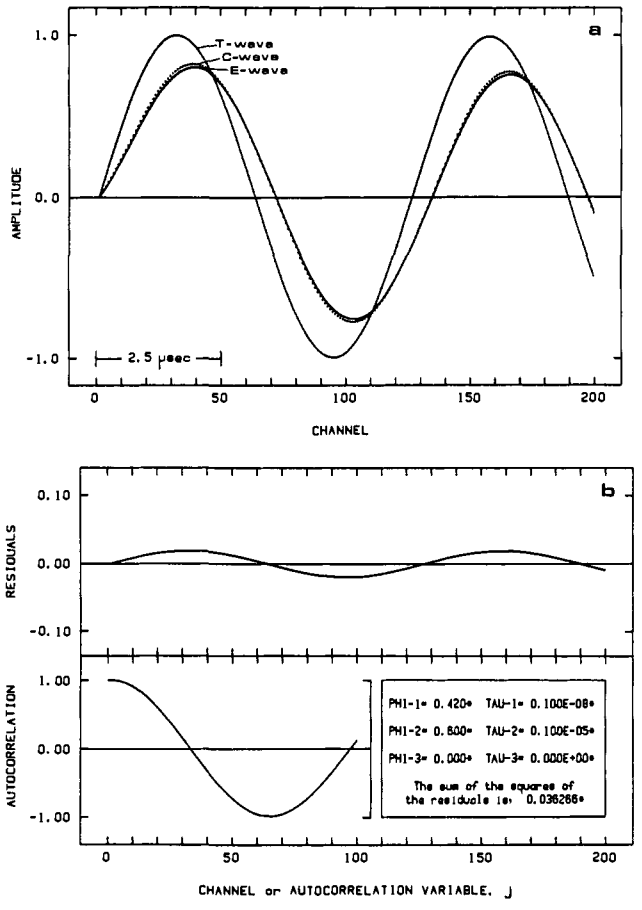

Figure 4. Model studies of waveform deconvolution. The T wave and E wave (solid lines) are identical with those of Figure 2. The C wave (dotted line) was calculated by using an incorrect choice for ϕ_1 (0.42 rather than 0.40). (a) Waveforms; (b) residuals and autocorrelation of residuals.

waveforms similar to those generated experimentally. In addition, the modeled waveforms can be treated within the computer program in a manner identical with that of the experimental waveforms, thus allowing model deconvolution studies. Equation 3 represents the mathematical convolution of one or more simultaneous transient decays with a transducer response. The computer program uses approximate algorithms to perform the same convolution. Thus, the accuracy of the computer program may be tested by comparing the computer convolution with the mathematical convolution.

Figure 2 shows the results of a model analysis involving two simultaneous transients. The impulse response T wave was generated by assigning $\phi_1 = 1.0$, $\tau_1 = 1$ ns in eq 3. (Letting $\tau_1 = 1$ ps or 1 fs would give the same result; Figure 1.) The E wave, representing two simultaneous transient decays, was generated by using eq 3 with $\phi_1 = 0.4$, $\tau_1 = 1$ ns, $\phi_2 = 0.6$, $\tau_2 = 1$ μs. Computer convolution using $\phi_1 = 0.4$, $\tau_1 = 1$ ns gave $c_1(i)$; convolution using $\phi_2 = 0.6$, $\tau_2 = 1$ μs gave $c_2(i)$, and the C wave was calculated by $C(i) = c_1(i) + c_2(i)$. Figure 2a shows the T wave, the E wave, c_1, c_2, and the C wave. The C wave is essentially superimposable with the E wave, but the differences in the two waves can be diagnosed by the autocorrelation of the residuals in Figure 2b. While the $\sum$res^2 is low (0.00002) and the residuals are not visually detectable on the −0.1 to 0.1 scale, the autocorrelation of the residuals indicates a nonrandom distribution of the residuals. (A good autocorrelation is represented by cor(0) = 1.0, cor(j) = 0.0 for $j \neq 0$.) Expansion of the residuals scale to −0.01 to 0.01, Figure 2c, shows a regular oscillation about the zero line, indicating that the C wave is shifted very slightly relative to the E wave. So, while the computer convolution algorithms do not give perfect results, the results are adequate. It has been found

(5) Rudzki, J. E. Ph.D. Thesis, Harvard University, 1985.

Table I. Results of Model Deconvolution Experiments

no. parameters varied	true value	final result[a]
1[b]	$\phi_1 = 0.60$	$\phi_1 = 0.60 \pm 0.01$
1[c]	$\tau_1 = 1.0$ ns	$\tau_1 < 5.9$ ns
	$\tau_1 = 10.0$ ns	$\tau_1 = 10.0 \pm 1.0$ ns
	$\tau_1 = 100$ ns	$\tau_1 = 97.4 \pm 5.3$ ns
	$\tau_1 = 500$ ns	$\tau_1 = 495 \pm 11$ ns
	$\tau_1 = 1$ μs	$\tau_1 = 0.99 \pm 0.04$ μs
	$\tau_1 = 25.0$ μs	$\tau_1 = 24.2 \pm 2.6$ μs
	$\tau_1 = 100$ μs	$\tau_1 = 103 \pm 6$ μs
2	$\phi_1 = 0.60$	$\phi_1 = 0.60 \pm 0.01$
	$\tau_1 = 1.0$ μs[c]	$\tau_1 = 0.99 \pm 0.01$ μs
3[b]	$\phi_1 = 0.4$	$\phi_1 = 0.40 \pm 0.03$
	$\phi_2 = 0.6$	$\phi_2 = 0.60 \pm 0.01$
	$\tau_2 = 1.0$ μs	$\tau_2 = 1.02 \pm 0.11$ μs

[a] Each result is reported as the value giving the lowest $\sum$res^2, along with a deviation representing those values bracketing the minimum in the search range. [b] $\tau_1 = 1$ ns. [c] $\phi_1 = 1.0$.

that the experiment-to-experiment fluctuations in the data are significantly greater than any systematic error in the curve-fitting process.

Figures 3 and 4 indicate how sensitive the waveforms and diagnostics are to an incorrect choice for a ϕ or τ value. In Figure 3, the T wave and E wave have been modeled by using parameters identical with those used for Figure 2. The C wave, however, was calculated by using an incorrect choice for τ_2: 1.1 μs rather than 1.0 μs. The result is a visible difference between the C wave and the E wave, detectable by the residuals on the −0.1 to 0.1 scale. The $\sum$res^2 in this case (0.07) is significantly higher than that for the correct choice of τ_2 (0.00002). In Figure 4, an incorrect choice was made for ϕ_1: 0.42 rather than 0.40. Again, a difference

Table II. Deconvolution Results of the Quenching of Triplet Benzophenone by 2,5-Dimethylhexa-2,4-diene following 337-nm Photoexcitation[a,b]

[diene], mM	ϕ_1	τ_1, ns	ϕ_2	τ_2, μs	$\phi_1 + \phi_2 + \phi_3$[b]
0.00	0.19 ± 0.01	1	0.74 ± 0.01	3.70 ± 0.01	[c]
0.20	0.19 ± 0.01	1	0.10 ± 0.01	0.52 ± 0.01	0.99 ± 0.02
0.33	0.19 ± 0.01	1	0.10 ± 0.01	0.34 ± 0.01	0.99 ± 0.02
1.00	0.18 ± 0.01	1	0.11 ± 0.01	0.12 ± 0.01	0.99 ± 0.02

[a] ϕ_n values are defined as the fraction of the photon energy (84.8 kcal/mol for 337-nm photoexcitation) released as heat for the relaxation process n. [b] For these calculations, $\tau_1 \equiv 1$ ns (the limit of the transducer resolution), $\phi_3 \equiv 0.70$,[11] and $\tau_3 \equiv 44$ ns.[15] [c] Only two sequential decays were assumed.

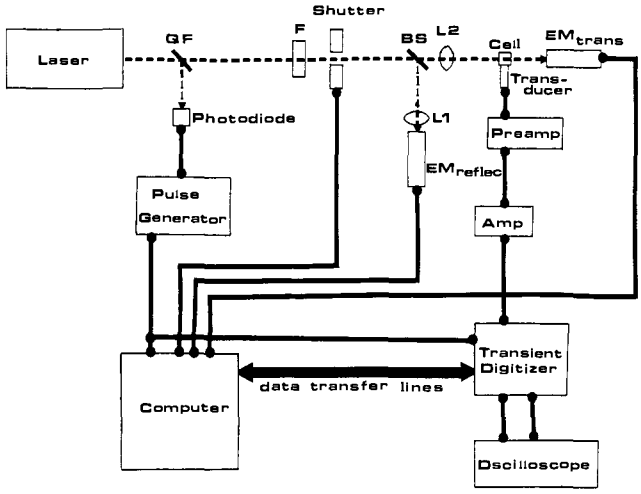

Figure 5. Schematic representation of the experimental apparatus. Dashed lines indicate light paths; thick solid lines represent signal paths. Abbreviations are the following: QF = quartz flat; F = filter; BS = beam splitter; L1, L2 = lenses; and EM = energy meter. L1 is a divergent lens which expands the beam into EM_{reflec}. The focus of L2 is between the cell and EM_{trans}. For simplicity, the trigger lines from the pulse generator to the two energy meters are not shown.

between the C wave and the E wave can be detected by visual inspection of the waveforms and the residuals, and the $\sum res^2$ is high (0.04).

Figures 2 through 4 indicate that the $\sum res^2$ is a sensitive indicator of the "quality of fit" of the C wave to the E wave. In general, a $\sum res^2$ value ≤ 0.001 indicates that the C wave is visually identical with the E wave. Computer model studies gave the deconvolution results shown in Table I.

V. Experimental Design

A schematic representation of the experimental arrangement is shown in Figure 5. Photoexcitation is achieved by the output of a nitrogen laser (Lumonics TE-261, 5-ns pulse, 337.1 nm) fired at a 3-Hz repetition rate. A fraction of the laser pulse is used to trigger the pulse generator (Hewlett-Packard 8013B) by means of a photodiode. The remainder of the laser pulse (~ 200 μJ) is attenuated by optical filters (Hoya) so that the pulse energy incident on the sample ranges from 2 to 20 μJ. A beam splitter (Oriel, 4494-1) directs ~30% of the laser output to the reference energy meter, EM_{reflec}, while the transmitted energy not absorbed by the sample cell is measured by the second energy meter, EM_{trans} (Laser Precision, Rj-7000 series with pyrolytic probes). The sample absorbance is determined for each laser shot in order that no photoproducts are produced that might interfere with the measurement. The response of the energy meter probes is improved by expanding the laser beam to fill the probe cavity. For this reason lenses L1 and L2 are used. L2 also serves to adjust the beam size incident on the sample cell to 2 mm in diameter.

The heat deposited by the photoinitiated event is detected by a piezoelectric element-based transducer,[1] clamped to the side of the cuvette with a layer of silicone grease interfacing the transducer and cuvette. The signal is amplified (Panametrics ultrasonic preamp and Princeton Applied Research 113 amplifier; gains of 10^4 (fixed) and ~10 (variable), respectively) and transferred to a transient digitzer (LeCroy WD8256). The digitizer is operated at 50 ns/channel with a full range of 1 V and an offset of −0.15 V. The offset is chosen so that the full wave (both positive and negative excursions) is digitized. Typically, data from 20 to 100 laser pulses are averaged to give one photoacoustic waveform. The data are collected and processed by a Digital MINC laboratory computer. The first 400 points of the acoustic waveform, as well as the energy meter values, are stored on floppy diskette and analyzed by deconvolution based on eq 1 and the theory of section III.

The quality of the data obtained in this experiment is highly dependent on keeping the parameter k in eq 1 as constant as possible throughout the experiment. Care is taken not to disturb the cuvette/transducer arrangement while changing samples. In addition, the experiments are performed as quickly as possible (typically in less than 30 min) to minimize the effects of random drift in the electronics and energy meter probe response.

The optical densities of the calibration compound and sample are normally adjusted to be within 2% of one another in order to avoid a difference in concentration gradient of heat-producing transients. For the experiments reported in this paper, the T wave was generated by photoexcitation of ferrocene. Ferrocene is apparently completely photoinert in solvents such as alkanes, acetone, and alcohols.[6] The photoacoustic behavior of ferrocene in comparison with other standards[1,4] is also consistent with the assignment of $\phi_h = 1.0$ for ferrocene and the assumption that the molecule relaxes back to ground state within 1 ns following photoexcitation. Samples were degassed by bubbling argon through them for several minutes and were maintained under argon atmosphere during data collection.

Scheme I

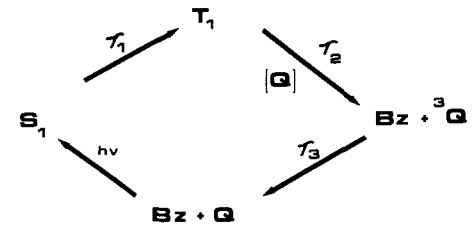

VI. Photochemical Systems

Quenching of the Benzophenone Triplet State by 2,5-Dimethylhexa-2,4-diene. Photoexcitation of benzophenone (Bz) results in the rapid formation (<6 ps) of the n−π* triplet state, T_1, via the singlet state, S_1, with unit efficiency,[7] Scheme I.

The benzophenone triplet can undergo triplet–triplet energy transfer with suitable quenchers. This process generates the triplet state of the quencher, ^3Q, which can then decay to its ground state. The rate constant for quenching, k_q, with dienes can be measured either directly[8] or more commonly by Stern–Volmer analysis.[9] Rates of quenching of the benzophenone T_1 by 2,5-dimethylhexa-2,4-diene (DMH) in acetonitrile were determined by using time-resolved photoacoustic calorimetry and then used to evaluate k_q by Stern–Volmer analysis.

Excitation of benzophenone in degassed acetonitrile solutions (0.2 OD, 337 nm, 300 K) in the presence of DMB (0–1 mM) generates an acoustic wave. By using ferrocene as the T-wave standard, deconvolution of the waveforms assuming three sequential decays, Scheme I, gave the results in Table II.[10] The values reported in Table II are the mean ± SD of the parameter values which gave rise to the lowest ten $\sum res^2$. The first rate is defined as $\tau_1 \equiv 1$ ns because the transducer cannot resolve heat

(6) Geoffroy, G. L.; Wrighton, M. S. "Organometallic Photochemistry"; Academic Press: New York, 1979; p 242.
(7) Turro, N. J. "Modern Molecular Photochemistry"; Benjamin/Cummings Co.: Menlo Park, CA, 1978; and references therein.
(8) Anderson, R. W.; Hochstrasser, R. M.; Lutz, H.; Scott, G. W. *J. Chem. Phys.* **1974**, *61*, 2500.
(9) (a) Stern, O.; Volmer, M. *Physik* **1919**, *20*, 183. (b) Reference 7, p 246.
(10) In the absence of quencher, only two sequential decays were assumed to deconvolve the waveforms.
(11) Murov, S. L. "Handbook of Photochemistry"; Marcel Dekker, Inc.: New York, 1973.

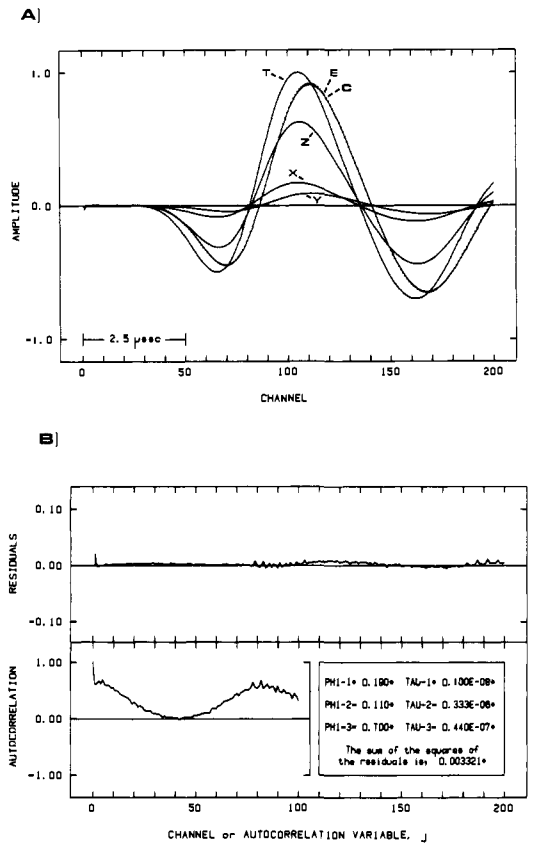

Figure 6. Deconvolution of the waveform from irradiation of benzophenone in acetonitrile with 0.33 mM DMH. (A) T wave—ferrocene; E wave (solid line)—benzophenone/DMH; C wave (dotted line)—convolution; X wave—first decay component; Y wave—second decay component; Z wave—third decay component. (B) Diagnostics of the convolution.

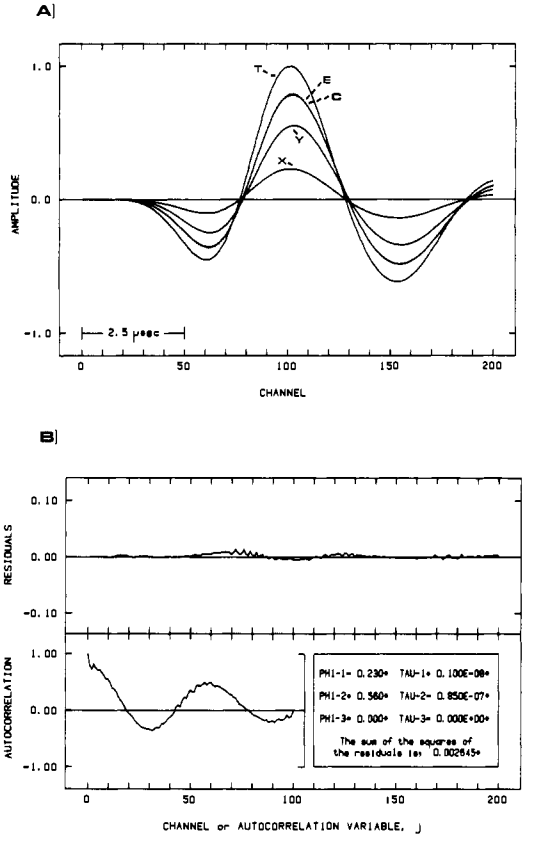

Figure 7. Deconvolution of the waveform from irradiation of valerophenone in ethanol. (A) T wave—ferrocene; E wave (solid line)—valerophenone; C wave (dotted line)—convolution; X wave—first decay component; Y wave—second decay component. (B) Diagnostics of the convolution.

Scheme II

depositions faster than ~5 ns. Thus, τ_1 may instead represent a ps heat deposition, for example. An example of the waveforms (T, E, and C waves) and the related diagnostics is given in Figure 6.

The first rate, $\tau \equiv 1$ ns, corresponds to the formation of the T_1 state of benzophenone. The energy of the state can be obtained from the relationship $E_T = E_{hv}(1 - \phi_1)$ where E_T is the energy of T_1, and E_{hv} is the photon energy (84.8 kcal/mol at 337 nm). The average value of $\phi_1 = 0.19$ gives a triplet energy of 69 kcal/mol, in excellent agreement with the literature value.[11] The second rate, τ_2, corresponds to the decay of T_1 by energy transfer to the diene and/or other processes. A Stern–Volmer plot of $1/\tau_2$ as a function of DMH concentration is linear ($r > 0.9999$) with a slope of 8.3×10^9 M^{-1} s^{-1} and an intercept of 2.5×10^5 s^{-1}. The slope corresponds to the bimolecular rate constant for quenching by DMH, k_q, and approaches the diffusion-controlled limit in acetonitrile. For comparison, the quenching of T_1 of benzophenone by *trans*-stilbene in acetonitrile occurs with $k_q = 7.5 \times 10^9$ M^{-1} s^{-1}.[12] The intercept indicates the lifetime of benzophenone in acetonitrile without quencher to be ~4 μs which agrees well with literature values.[13] The value $(\phi_2)E_{hv}$ is the energy difference between the triplet states of benzophenone and DMH, ~9.3 kcal/mol.[14] The third rate, $\tau_3 = 44$ ns, which was not determined but rather taken from the literature,[15] corresponds to the decay of the triplet state of DMH. The value $(\phi_3)E_{hv}$ is the triplet energy of DMH, ~59 kcal/mol.[11] At all diene concentrations employed, $\phi_1 + \phi_2 + \phi_3 \simeq 1.0$, thus accounting for all of the photon energy. This implies that energy transfer from T_1 to DMH does not produce any long-lived intermediates, detectable by their energetics, at these diene concentrations.[16,17]

Norrish Type II Photocleavage of Valerophenone. Upon photoexcitation, valerophenone undergoes intersystem crossing with unit efficiency from S_1 to T_1. The T_1 state rapidly undergoes intramolecular hydrogen abstraction to form a triplet 1,4-biradical.[18] The 1,4-biradical then cleaves to form propene and acetophenone, initially via its enol, Scheme II. Time-resolved photoacoustic calorimetry was used to investigate the kinetics and energetics of the triplet 1,4-biradical.

Excitation of valerophenone in ethanol (0.2 OD, 337 nm, 300 K) gave a waveform which was deconvoluted with ferrocene as the T-wave standard. The waveforms (T, E, C waves) and the deconvolution parameter values obtained assuming two sequential decays are given in Figure 7.[19] The first rate, $\tau_1 \equiv 1$ ns, corresponds to the formation of the 1,4-biradical.[20] The value of $E_{hv}(1 - \phi_1)$ gives the energy of the triplet biradical above the ground-state species. The value obtained, 65 ± 3 kcal/mol, is lower than that expected from bond energy considerations;[21] however, this may

(12) Clark, W. D.; Steel, C. *J. Am. Chem. Soc.* **1971**, *93*, 6347.
(13) (a) Clark, W. D.; Litt, A. D.; Steel, C. *J. Am. Chem. Soc.* **1969**, *91*, 5413. (b) Giering, L.; Berger, M.; Steel, C. *J. Am. Chem. Soc.* **1974**, *96*, 953.
(14) From the literature (ref 11), E_T(benzophenone) − E_T(DMH) ≃ 10 kcal/mol.
(15) Caldwell, R. A.; Singh, M. *J. Am. Chem. Soc.* **1982**, *104*, 6121.
(16) Deconvolution of the DMH quenching data with use of only two decays gave similar results. The τ'_2 and ϕ'_2 obtained were essentially equal to $(\tau_2 + \tau_3)$ and $(\phi_2 + \phi_3)$, respectively, obtained from the three sequential decay fit. This appears reasonable given $\tau_2 \gg \tau_3$. The k_q from Stern–Volmer analysis with use of two sequential decays was 6.2×10^9 M^{-1} s^{-1}.
(17) This is in contrast to the quenching of T_1 of benzophenone by 1,3-cyclohexadiene where a long-lived intermediate is observed after energy transfer. The long-lived intermediate is most probably the triplet state of the diene which has a lifetime[15] of 1.3 μs, much longer than that of DMH, 44 ns.
(18) Wagner, P. J. *Acc. Chem. Res.* **1971**, *4*, 168 and references therein.
(19) The experiment was run several times and the parameter values obtained were similar to those in Figure 7. The reported values are calculated as the mean ± SD of the experimental results.

be due to the stabilizing effect of the hydrogen-bonding solvent.[22] The effect of solvent and substitution on the energy of this triplet biradical will be addressed in a subsequent paper. The second rate, $\tau = 85 \pm 10$ ns, corresponds to the cleavage of the 1,4-biradical and is in good agreement with the value obtained by Caldwell,[23] 93 ns, using nanosecond absorption spectroscopy. The enthalpy of reaction, ΔH_r, for the photocleavage of valerophenone to acetophenone and propene is given by $\Delta H_r = E_{h\nu}(1 - \phi_1 - \phi_2)$. The experimental enthalpy of reaction, 18 ± 6 kcal/mol, approximates the value obtained from thermochemical calculations.[24,25]

Conclusion

Pulsed time-resolved photoacoustic calorimetry can be used to obtain both kinetic and thermodynamic information. This technique has been applied to two simple chemical systems: the quenching of the T_1 state of benzophenone by DMH and the Norrish type II photocleavage of valerophenone. It remains to be seen what degree of complexity can be handled by this technique in a believable fashion. One of the major strong points of this method is that reactions having intermediates without chromophores can be studied, in terms of both kinetics and energetics. Ultimately, it is only the judicious interpretation of the kinetic and thermodynamic data that will demonstrate the future utility of this technique.

Acknowledgment. This work was supported by a grant from the Petroleum Research Fund, administered by the American Chemical Society. K.S.P. acknowledges support from the Alfred P. Sloan Foundation and the Henry and Camille Dreyfus Foundation for a teacher-scholar grant. J.L.G. acknowledges generous support from an NIH postdoctoral fellowship.

Registry No. Benzophenone, 119-61-9; 2,5-dimethylhexa-2,4-diene, 764-13-6; valerophenone, 1009-14-9.

(20) Although the formation of the 1,4-biradical from T_1 of valerophenone is actually longer,[18] 8 ns, than indicated, separating the τ_1 into two sequential decays does not change the deconvolution results significantly. In fact, 8 ns is at the limit of the resolution of the transducer.

(21) Using D(H–CH(OH)(C_6H_5)) = 81.2 kcal/mol, D(H–CH(CH_3)$_2$) = 97.9 kcal/mol, and D(H–H) = 104 kcal/mol,[22] then the energy of the 1,4-biradical can be crudely estimated to be ~75 kcal/mol.

(22) McMillen, D. F.; Golden, D. M. *Annu. Rev. Phys. Chem.* **1982**, *33*, 493.

(23) Caldwell, R. A.; Majima, T.; Pac, C. *J. Am. Chem. Soc.* **1982**, *104*, 629.

(24) Using $\Delta H_f°$(acetophenone, l) = −34.07 kcal/mol, $\Delta H_f°$(propene, g) = +4.88 kcal/mol, and assuming $\Delta H_f°$(valerophenone, l) = $\Delta H_f°$(isobutyl phenyl ketone, l) = −52.63 kcal/mol, then ΔH_r = 23.4 kcal/mol.[26]

(25) It is assumed that the enol of acetophenone tautomerizes rapidly under the reaction conditions. The free energy differences between the enol and acetophenone is ~5.5 kcal/mol at 300 K.[27] The small energy release due to tautomerization would be difficult to detect with the present experimental design.

(26) See: Cox, J. D.; Pilcher, G. "Thermochemistry of Organic and Organometallic Compounds"; Academic Press: New York, 1970.

(27) Gero, A. *J. Org. Chem.* **1954**, *19*, 1960.

Factors Determining CO Adsorption Sites on Pd and Pt (100) and (111) Surfaces: Theoretical Study

Alfred B. Anderson* and Md. K. Awad

Contribution from the Chemistry Department, Case Western Reserve University, Cleveland, Ohio 44106. *Received July 1, 1985*

Abstract: The atom superposition and electron delocalization molecular orbital theory and two-layer thick cluster models are used to predict the binding site preferences and bond lengths of CO on Pd(111) and -(100) and Pt(100) surfaces. Binding at 3-fold sites is predicted to be favored for Pd(111) and at 2-fold sites for Pd(100). These results are supported by the experimental literature. The difference between Pd and Pt vis-â-vis CO adsorption is shown to depend solely on the position of the metal valence bands: the Pd valence band lies about 1 eV higher in energy and the resulting enhancement of surface back-donation to the empty CO π^* orbitals favors higher coordination sites than on the Pt surfaces. Metal orbital size and surface atom spacing differences are insufficient to alter the dominance of the band positions on these results. The dependence of CO adsorption on Pd and Pt valence band positions is used as a basis for extrapolating to the effects of electropositive and electronegative coadsorbates and electrochemical charging of CO covered surfaces in electrolytes.

It is well established by a variety of experimental techniques that carbon monoxide binds predominately to 1-fold sites (always standing vertically, carbon end down) on Pt(111)[1] and to 3-fold sites on Pd(111)[2] at low coverage. Further, an analogous tendency exists for the (100) surfaces where 1-fold and 2-fold coordinations are seen on Pt[3] but 2-fold alone is seen on Pd.[2,3d,4] The question of why these differences exist naturally arises. An argument to explain this which considers the metal atom size was considered but found inadequate.[3c] One suggestive result lies in the work of Garfunkel et al.[1d] showing a shift of CO from 1-fold to 2-fold and possibly 3-fold sites on Pt(111) on increasing the coverage of coadsorbed potassium atoms. Ray and Anderson explained this result by using molecular orbital theory.[5] They predicted the shift of CO to higher coordinate sites to take place as a result of the destabilization (shifting up in energy) of the Pt valance band due to charge transfer from the coadsorbed potassium. This shift of the metal valence band closer in energy to the empty CO π^* orbital energy levels leads to increased π^* orbital mixing with and stabilization of Pt d band orbitals and decreased donation stabilization from the CO 5 σ orbital which lies beneath the Pt valence band. As Ray and Anderson show, strong π^* mixing favors high coordinate sites and strong 5 σ mixing favors the 1-fold site on Pt(111), which explains the shift to high coordinate sites when CO and K are coadsorbed. The 4d ionization potential of the Pd atom is about 1 eV less than the 5d ionization potential of the

(1) (a) H. Froitzheim, H. Hopster, H. Ibach, and J. Lehwald, *Appl. Phys.*, **13**, 147 (1977). (b) H. I. Krebs and H. Luth, *Appl. Phys.*, **14**, 337 (1977). (c) P. R. Norton, J. W. Goodale, and E. B. Selkirk, *Surf. Sci.*, **83**, 189 (1979). (d) E. L. Garfunkel, J. E. Crowell, and G. A. Somorjai, *J. Phys. Chem.* **86**, 310 (1982).

(2) A. M. Bradshaw and F. M. Hoffmann, *Surf. Sci.*, **72**, 513 (1978). (b) A. Brown and J. C. Vickerman, *Surf. Sci.*, **124**, 267 (1983).

(3) (a) S. Andersson, *Solid State Commun.*, **21**, 75 (1977). (b) G. Broden, G. Pirug, and H. P. Bonzel, *Surf. Sci.*, **72**, 45 (1978). (c) A. Crossley and D. A. King, *Surf. Sci.*, **95**, 131 (1980). (d) J. P. Biberian and M. A. Van Hove, *Surf. Sci.*, **118**, 443 (1982).

(4) (a) R. L. Park and H. H. Madden, *Surf. Sci.*, **11**, 158 (1968). (b) H. Conrad, G. Ertl, J. Koch, and E. E. Latta, *Surf. Sci.*, **43**, 462 (1974). (c) R. J. Behm, K. Christmann, G. Ertl, M. A. Van Hove, P. A. Thiel, and W. H. Weinberg, *Surf. Sci.*, **88**, L59 (1979). (d) A. Ortega, F. M. Hoffmann, and A. M. Bradshaw, *Surf. Sci.*, **119**, 79 (1982). (e) A. Brown and J. C. Vickerman, Surf. Sci. *151*, 319 (1985).

(5) N. K. Ray and A. B. Anderson, *Surf. Sci.*, **125**, 803 (1983).

0002-7863/85/1507-7854$01.50/0